The vertical spanning strip wall as a coupled rocking rigid body assembly

Luigi Sorrentino[†] and Renato Masiani[‡]

Structural and Geotechnical Engineering Department, Sapienza University, Rome, Italy

Michael C. Griffith[‡†]

School of Civil, Environmental and Mining Engineering, The University of Adelaide, Adelaide, South Australia, Australia

Abstract. The equation of motion of a one way (vertical) spanning strip wall, as an assembly of two rigid bodies, is presented. Only one degree of freedom is needed to completely describe the wall response as the bodies are assumed to be perfectly rectangular and are allowed to rock but not to slide horizontally. Furthermore, no arching action occurs since vertical motion of the upper body is not restrained. Consequently, the equation of motion is nonlinear, with non constant coefficients and a Coriolis acceleration term. Phenomena associated with overburden to self weight ratio, motion triggering, impulsive energy dissipation, amplitude dependency of damping and period of vibration, and scale effect are discussed, contributing to a more complete understanding of experimental observations and to an estimation of system parameters based on the wall characteristics, such as intermediate hinge height and energy damping, necessary to perform nonlinear time history analyses. A comparison to a simple standing, or parapet, wall is developed in order to better highlight the characteristics of this assembly.

Keywords: rocking response; threshold acceleration; impulsive energy dissipation; amplitude dependency; scale effect.

1. Introduction

The dynamic behaviour of a kinematic chain, made up by two rectangular bodies, is presented. Body and foundation deformabilities are neglected and the friction between the bodies as well as between the system and both the ground and the top restraint is assumed to be sufficient to prevent horizontal sliding. Complete loss of contact between the bodies and/or the supports is not permitted and the top roller support is assumed to be in synchronous motion with the ground support so that the system can be represented as a single degree of freedom (SDOF) system, an assumption which is reasonable if the diaphragms are not too flexible. Further, the top restraint does not hinder the vertical motion of the upper body and uniform mass density distribution is assumed so that the

† Ph.D., Corresponding author, E-mail: luigi.sorrentino@uniroma1.it
‡ Professor, E-mail: renato.masiani@uniroma1.it
‡† Associate Professor, E-mail: mcgrif@civeng.adelaide.edu.au

centre of mass and geometric centroid is coincident for each body. The displacements are also considered to be finite.

On a previous occasion (Sorrentino and Masiani 2003), it has been qualitatively shown, by means of field and laboratory evidence, that a model based on the previous hypotheses can effectively represent a vertical spanning strip wall (VSSW) subject to out-of-plane earthquake induced inertia forces. A VSSW is intended to represent a wall with significant restraint on top due to connection to floor or roof system and negligible lateral restraint due to inadequate connection to lateral walls or to the existence of openings. This mechanism can prove dangerous for wall aspect ratios (i.e., height over thickness) exceeding 12-14. Such values can be common in contemporary masonry buildings as well as in premodern edifices with large halls such as churches, school gyms, and theatres.

The first to develop an analytical model to reproduce the dynamic response of one way spanning unreinforced concrete and dry stacked masonry specimens were Baggio and Masiani (1991). However, the matrix equation of motion they presented was valid only for small displacements. Possibly the widest experimental campaign on the matter was that performed by Ewing, Johnson and Kariotis as part of the Agbabian, Barnes and Kariotis consortium (ABK 1981, 1984), whose brick and block walls did not necessarily collapse after cracking and rocking. Recent laboratory tests on this issue were carried out by Doherty and Griffith (Doherty 2000, Doherty *et al.* 2002, Griffith *et al.* 2003, 2004, Lam *et al.* 2003). The authors numerically reproduced the test results using an equivalent elastic nonlinear SDOF oscillator, with experimentally established stiffness and viscous damping, valid for an intermediate hinge at mid height.

Simsir *et al.* (2004) experimentally accounted for the effect of stiff or flexible diaphragms, noting in the second case an increase in the out-of-plane wall displacements and mechanism periods. Intermediate cracking was observed only when superimposed load was reduced compared to wall self weight, a condition which is typical of top storeys façades. The intermediate hinge has formed around 70% of the wall height. In their laboratory tests on full-scale models, Meisl *et al.* (2006) considered the influence of different ground motions and quality of construction. Rocking of a coupled-rigid body assembly was observed even though the specimens were three-wythe walls and, in two out of four cases, poor quality workmanship. The intermediate hinge height spanned between 65 and 74% of the wall height. Wilhelm *et al.* (2007) tested different boundary conditions: if this is fixed at the top (neither rotation nor elongation allowed) no rocking was observed because of arch action. The use of a low flexural strength mortar caused the opening of multiple cracks in the upper third of the wall, with a major crack moving down from the top of the wall and back up again.

In the following pages first the kinematics of the model will be described (§ 2); then, using a Lagrangian approach, the equation of motion will be introduced (§ 3); subsequently motion triggering and intermediate hinge height will be addressed (§ 4); energy dissipation will be introduced and discussed (§ 5); amplitude dependency of energy dissipation and period of vibration will be highlighted (§ 6); finally sample response and scale effect will be presented (§ 7).

2. System kinematics, potential and kinetic energies, contribution of external forces

Under the previously stated assumptions, and neglecting for the time being mass and inertia related terms, the geometry of the system under consideration is fully described when a set of three parameters is known. These are either b, h_1 and h_2, or α_1, α_2 and R_1, as shown in Fig. 1 where b is
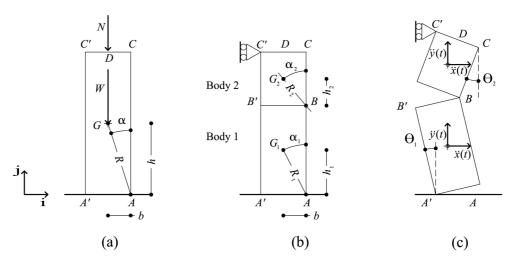
Fig. 1 (a) Uncracked wall parameters and reference axes, (b) cracked vertical spanning strip wall parameters, (c) displaced configuration and ground acceleration components acting in the mass centres of the two bodies

the half-thickness of the two bodies; h_1 and h_2 are the half-height of the lower, from now on denoted with the subscript $_1$, and the upper, subscript $_2$, bodies. Half instead of full dimensions are used following the study of a single rocking body (Housner 1963) where this made the closed form solution of the linearised free vibrations equation more compact. α_1 and α_2 are the angles formed by the vertical line passing through the base corner and the segment between this point and the respective mass centre G_i, the length of such segment in the body 1 being R_1; the first two values determine the shape (i.e., height to thickness ratio) of the system, while the third fixes its size.

The choice of the group of three variables is arbitrary: the first is more directly related to the measures of a given wall, however the second is in agreement with previous research on rocking bodies and, as will be shown, in some situations reduces by one the number of geometrical parameters. Consequently, the latter will be ordinarily used, although in order to refer to the height of the intermediate hinge (§ 4) the dimensionless height h_1/h, where $h = h_1 + h_2$ is the half height of the whole system, will be preferred. Typical values in building practice for the above parameters can be found in Table 1 and derive from the experimental data reported in ABK (1981).

Because any top support or base foundation flexibility has been neglected (Koh *et al.* 1986, Spanos and Koh 1986), the only Lagrangian coordinate of the system is the rotation θ_1 of the lower body, taken positive if in the anticlockwise direction. Therefore, the finite displacements $\mathbf{s}_{G,1}$ and $\mathbf{s}_{G,2}$, of the respective centres of mass G_1 and G_2, are (refer to Fig. 1(c))

$$\mathbf{s}_{G,1} = -R_1\sin(\alpha_1 - \theta_1)\mathbf{i} + R_1\cos(\alpha_1 - \theta_1)\mathbf{j} \tag{1a}$$

$$\mathbf{s}_{G,2} = -[2R_1\sin(\alpha_1 - \theta_1) - R_2\sin(\alpha_2 + \theta_2)]\mathbf{i} + [2R_1\cos(\alpha_1 - \theta_1) + R_2\cos(\alpha_2 + \theta_2)]\mathbf{j} \tag{1b}$$

where $\mathbf{i}$ and $\mathbf{j}$ are unit vectors parallel to the horizontal and vertical axes, respectively. Similarly it is possible to obtain the displacement of the point of the upper face of the system, where a concentrated force N is acting.

Since the system has only one independent DOF, the rotation θ_2 can be expressed as a function of θ_1

Table 1 Geometric data from dynamic experimental tests on vertical spanning strip walls (ABK 1981)

Specimen	Height (m)	Thickness (m)	h_1/h	α_1/α_2	α_1	R_1 (m)
1	4.88	0.356	0.69	0.46	0.11	1.69
2	4.88	0.356	0.64	0.57	0.11	1.57
3	4.88	0.356	0.54*	0.85	0.13	1.33
4^						
5	3.05	0.143	0.53	0.89	0.09	0.81
6	3.05	0.143	0.67	0.50	0.07	1.02
7	4.88	0.200	0.50	1.00	0.08	1.22
8	4.88	0.200	0.54	0.85	0.08	1.32
9	4.88	0.200	0.46	1.17	0.09	1.13
10	4.88	0.194	0.75	0.34	0.05	1.83
11	4.88	0.194	0.67	0.49	0.06	1.64
12^						
13	3.05	0.194	0.53	0.89	0.12	0.81
14	3.05	0.194	0.63*	0.59	0.10	0.97
15	3.05	0.194	0.60	0.67	0.11	0.92
16	3.05	0.143	0.67	0.50	0.07	1.02
17	3.05	0.143	0.60+	0.67	0.08	0.92
18	3.05	0.143	0.60	0.67	0.08	0.92

^ discharged because damaged
+ fractured, during transportation, at $h_1/h = 0.87$
* hinge position varied during tests
# homogeneity assumed

$$\theta_2 = \text{sgn}(\theta_1)\left\{\arcsin\left[\frac{\sin\alpha_2}{\sin\alpha_1}\sin(\alpha_1 - |\theta_1|)\right] - \alpha_2\right\} \qquad (2)$$

valid no matter what the sign of θ_1 is. This equation is valid until the top roller support is violated, a condition that under transient excitations is usually experienced just prior to the complete overturning, or when the no penetration condition between the bodies is violated, a circumstance theoretically possible only for very stubby (large $\alpha_i = \arctan b/h_i$) blocks.

It is possible to numerically show that Eq. (2) can be linearised by the following

$$\theta_2 = -\frac{\tan\alpha_2}{\tan\alpha_1}\theta_1 \qquad (3)$$

with appreciable differences only for very large rotations ($\theta_1 > \alpha_1$) and only for α_1 and α_1/α_2 values outside the range encountered in the practice (ABK 1981, Doherty 2000). Thus, in the framework of the other simplified assumptions Eq. (3) will be preferred to Eq. (2). Finally no approximation at all exists if the two angles are equal (i.e., $h_1 = h_2$ or crack is at mid-height).

The angular velocity of the upper body, $\dot\theta_2$, as a function of $\dot\theta_1$ is

$$\dot\theta_2 = -\frac{\sin\alpha_2}{\sin\alpha_1}\frac{\cos(\alpha_1 - \theta_1)}{\cos(\alpha_2 + \theta_2)}\dot\theta_1 \qquad (4)$$
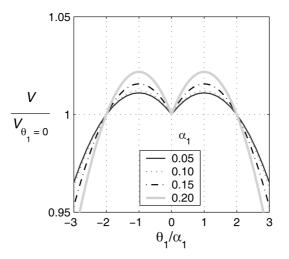
Fig. 2 Non dimensional potential energy as a function of non dimensional rotation. $\alpha_2 = 0.225$ rad

which is dependent on the amplitude of the angular displacement. For a positive rotation of body 1, the velocities, $\mathbf{v}_{G,1}$ and $\mathbf{v}_{G,2}$, of the respective centres of mass are

$$\mathbf{v}_{G,1} = -R_1[\cos(\alpha_1 - \theta_1)\mathbf{i} - \sin(\alpha_1 - \theta_1)\mathbf{j}]\dot{\theta}_1 \qquad (5a)$$

$$\mathbf{v}_{G,2} = -R_1\left\{\cos(\alpha_1 - \theta_1)\mathbf{i} - \left[2\sin(\alpha_1 - \theta_1) + \frac{\cos(\alpha_1 - \theta_1)}{\cot(\alpha_2 + \theta_2)}\right]\mathbf{j}\right\}\dot{\theta}_1 \qquad (5b)$$

Following Eqs. (1a-b) and (5a-b) the potential, V, and kinetic, Z, energies are respectively

$$V = R_1 g\left[(m_1 + 2m_2)\cos(\alpha_1 - \theta_1) + m_2\frac{\sin\alpha_1}{\sin\alpha_2}\cos(\alpha_2 + \theta_2)\right] \qquad (6)$$

$$Z = \frac{1}{2}R_1^2\left\{m_1 + m_2\left\{\cos^2(\alpha_1 - \theta_1) + \sin^2(\alpha_1 - \theta_1)\left[2 + \frac{\tan(\alpha_2 + \theta_2)}{\tan(\alpha_1 - \theta_1)}\right]^2\right\} + \frac{1}{R_1^2}\left[I_{G,1} + \frac{\sin^2\alpha_2}{\sin^2\alpha_1}\frac{\cos^2(\alpha_1 - \theta_1)}{\cos^2(\alpha_2 + \theta_2)}I_{G,2}\right]\right\}\dot{\theta}_1^2 \qquad (7)$$

with m mass, I_G polar moment of inertia with reference to the mass centre, g gravity acceleration. It should be noted that as before, the subscripts 1 and 2 refer to the lower and upper bodies, respectively. Since the ground has been assumed as a reference for the heights of the mass centres, the potential energy is positive when the system is at rest ($\theta_1 = 0$). A plot of Eq. (6) is presented in Fig. 2. The potential energy of the system under examination is qualitatively similar to that of a rocking single body: it has a local minimum corresponding to the rest position ($\theta_1 = 0$), a maximum for the non dimensional rotation equal to one ($\theta_1 = \alpha_1$) and then decreases until the rotation is incompatible with the top restraint boundary condition (not shown in the Figure). As is well known, the maximum for $\theta_1 = \alpha_1$ corresponds to a point of static instability: therefore, a system with zero

initial velocity and no driving force, released with a rotation higher than α_1, will experience no vibration but simply migrate toward another configuration. However, if forced vibrations are considered non dimensional rotations θ_1/α_1 higher than unity are possible, although in the numerical analyses performed only values slightly exceeding one were observed without overturning.

The work done by the superimposed gravity load N, applied to the upper body (refer to Fig. 1), in terms of virtual work $\delta\Gamma_N$ for a positive infinitesimal rotation of the lower body $\delta\theta_1$ is

$$\delta\Gamma_N = -NR_1\left\{2\sin(\alpha_1 - \theta_1) + \tan\alpha_2\cos\alpha_1\left(\cos\theta_2 + 2\frac{\sin\theta_2}{\tan\alpha_2}\right)\right\}\delta\theta_1 \tag{8}$$

There is experimental evidence (ABK 1981, Doherty 2000) that the gravity load N can migrate toward the upper corner of body 2 if no special connection details are used (Simsir *et al.* 2004). However, it is usual (Giuffrè 1993) and conservative to assume that the gravity load N acts at the wall's centreline, as will be done in the following.

The contribution of inertia forces, acting in the two mass centres and proportional to a ground acceleration varying with time t, whose horizontal and vertical components are $\ddot{x}(t)$ and $\ddot{y}(t)$ respectively (see Fig. 1(c)), for a positive rotation of the lower body, in terms of virtual work is equal to

$$\delta\Gamma = R_1\left\{-\ddot{x}(t)\left[(m_1 + 2m_2)\cos(\alpha_1 - \theta_1) - m_2\frac{\cos\alpha_1}{\cos\alpha_2}\cos(\alpha_2 + \theta_2)\right] + \right.$$
$$\left. \text{sgn}(\theta_1)\ddot{y}(t)\left[(m_1 + 2m_2)\sin(\alpha_1 - \theta_1) + m_2\frac{\cos\alpha_1}{\cos\alpha_2}\sin(\alpha_2 + \theta_2)\right]\right\}\delta\theta_1 \tag{9}$$

The assumption behind Eq. (9) is that the accelerations at the ground and at the top roller support are identical, an assumption not too far from reality if diaphragms are not too flexible (Simsir *et al.* 2004, Meisl *et al.* 2006). Moreover, ABK (1981, 1984) after the most extensive experimental campaign to date, sustained that the overturning of a VSSW was more than usually not related to asynchrony in the motions of ground and top support. Additionally, to model how a ground shaking could be filtered all the way up to the roller support in C' the consideration of many more variables and, consequently, uncertainties would be required. Thus, the preceding assumption will be taken in the rest of the paper and Eq. (9) used.

3. Equation of motion

Based on Eqs. (6)-(9) the equation of motion for forced vibrations is equal to

$$R_1C_A\ddot{\theta}_1 + \text{sgn}(\theta_1)R_1C_S\dot{\theta}_1^2 = -\ddot{x}(t)C_H + \text{sgn}(\theta_1)[\ddot{y}(t) - g]C_V - \text{sgn}(\theta_1)NC_N \tag{10}$$

with

$$C_A = m_1 + m_2\left[\cos^2A_1 + \sin^2A_1\left(2 + \frac{\tan A_2}{\tan A_1}\right)^2\right] + \frac{1}{R_1^2}\left(I_{G,1} + \frac{\sin^2\alpha_2\cos^2A_1}{\sin^2\alpha_1\cos^2A_2}I_{G,2}\right) \tag{11a}$$

$$C_S = \frac{1}{R_1^2}\cos A_1 \frac{\sin^2\alpha_2}{\sin^2\alpha_1}\sec^2 A_2 \Big(\sin A_1 - \cos A_1 \frac{\tan\alpha_2}{\tan\alpha_1}\tan A_2 \Big) I_{G,2} +$$

$$m_2 \sin A_1 \Big\{ \cos A_1 \Big[1 - \Big(2 + \frac{\tan A_2}{\tan A_1} \Big)^2 \Big] + \tag{11b}$$

$$\sin A_1 \Big(2 + \frac{\tan A_2}{\tan A_1} \Big)\Big(-\frac{\tan\alpha_2}{\tan\alpha_1}\cot A_1 \sec^2 A_2 + \csc^2 A_1 \tan A_2 \Big) \Big\}$$

$$C_H = (m_1 + 2m_2)\cos A_1 - m_2 \frac{\cos\alpha_1}{\cos\alpha_2}\cos A_2 \tag{11c}$$

$$C_V = (m_1 + 2m_2)\sin A_1 + m_2 \frac{\cos\alpha_1}{\cos\alpha_2}\sin A_2 \tag{11d}$$

$$C_N = 2\sin A_1 + \tan\alpha_2\cos\alpha_1 \left[\cos\Big(\frac{\tan\alpha_2}{\tan\alpha_1}|\theta_1|\Big) - \frac{2\sin\Big(\frac{\tan\alpha_2}{\tan\alpha_1}|\theta_1|\Big)}{\tan\alpha_2} \right] \tag{11e}$$

and $A_1 = \alpha_1 - |\theta_1|$, $A_2 = \alpha_2 - \frac{\tan\alpha_2}{\tan\alpha_1}|\theta_1|$.

Considering Eq. (10), it is possible to note that all the system coefficients are not constant, since C_A, C_S, C_H, C_V and C_N, are functions of rotation θ_1. Moreover, a Coriolis effect, due to the vertical slide-rotation of the upper body, is detectable too. In Eq. (10) angular acceleration and velocity appear explicitly; however, the angular displacement is present in a non algebraic form. No progressive damage is considered in the model, since this is usually negligible (Doherty 2000, Simsir *et al.* 2004, Wilhelm *et al.* 2007) unless construction quality is very poor (Meisl *et al.* 2006). Finally, as already stated, no energy damping term is yet included in the equation of motion. The issue will be addressed in § 5.

4. Threshold acceleration and intermediate hinge height

As for other rocking systems (Spanos and Koh 1984, Allen *et al.* 1986, Psycharis 1990, Oppenheim 1992, Sinopoli and Sepe 1993, Spanos *et al.* 2001), it is possible to recognize as a system feature a threshold acceleration $\ddot{x}_t$: an acceleration that triggers the motion. This, irrespective of the sign of the acceleration, is equal to

$$|\ddot{x}_t(t)| = \tan\alpha_1 \frac{[g - \ddot{y}(t)]\Big[m_1 + \Big(m_2 + \frac{N}{g} \Big)\Big(2 + \frac{\tan\alpha_2}{\tan\alpha_1} \Big) \Big]}{m_1 + m_2} \tag{12}$$

which is obtained from Eq. (10) by setting the angular displacement, velocity and acceleration equal to zero. In the case of homogeneous bodies without a gravity load N, Eq. (12) can be simplified to

$$|\ddot{x}_t(t)| = 2[g - \ddot{y}(t)]\tan\alpha_1 \tag{13}$$

It can be observed from Eq. (13), presented in a slightly different form in Wilhelm *et al.* (2007), that the threshold acceleration is not a function of the size of the system, as experimentally confirmed for other assemblies (Winkler *et al.* 1995).

However, the perfect parallelepiped assumption usually leads to overestimation of the threshold acceleration (Ishiyama 1984), and is not feasible to fully reproduce experimental time histories of masonry walls or even rigid blocks, at least if no special experimental setting is used (Tso and Wong 1989). This can be stated also for the particular case considered here. Making reference e.g., to Figs. 5.18 and Figs. 5.20 in ABK (1981), plotted under synchronous motion of both supports, rocking was observed before the theoretical threshold acceleration was reached. However, in the same research campaign cracking of the wall and formation of the intermediate hinge was not recorded under some strong motion, therefore showing that a certain minimum acceleration is indeed necessary to set the system into rocking.

Setting equal to zero the vertical component of the ground acceleration, considering homogenous bodies and expressing Eq. (12) as a function of *b*, *h* and h_1, one gets

$$\left|\frac{\ddot{x}_t}{g}\right| = \frac{b\xi}{h-h_1} + \frac{2b(1+\xi)}{h_1} \tag{14}$$

with $\xi = N/W$, and *W* weight of the whole wall. Eq. (14) represents the static collapse load multiplier of the mechanism considered. The non dimensional height h_1/h that minimizes the threshold acceleration of Eq. (14) is

$$\frac{h_1}{h} = \frac{1}{1 + \sqrt{\dfrac{\xi}{2(1+\xi)}}} \tag{15}$$

Both Eq. (14) and Eq. (15) were presented, although in a slightly different form, in Giuffrè (1993). The latter clearly states that the height of the intermediate hinge is a function of the sole non dimensional load ξ: the higher ξ the lower h_1/h. Such a trend was confirmed by static experimental tests, using a tilting table, on dry stacked stone masonry walls (Giuffrè 1993). It is perhaps interesting to note that, for $\xi \to \infty : h_1/h \to 2-\sqrt{2} \cong 0.5858$. Although a very small amount of non dimensional superimposed load is enough to lower its position, on the other hand if ξ tends to zero the hinge tends to form at the very top of the system. There have only been a few tests conducted without superimposed load. Meisl *et al.* (2006), whose specimens were built placing brick units dry in order to create a weak bond with the mortar, reported interference of the top restraint and a dislodged row of bricks due to limited moment resistance at the top of the wall. Wilhelm *et al.* (2007) observed multiple cracks in the upper third of the wall and a major crack moving down from top of the wall and back up. However, if average to good quality mortar is present the intermediate crack is usually far from the top of the wall (Gülkan *et al.* 1979, ABK 1981, Anderson and Held 1982, Doherty 2000).

Let us consider the wall as a beam clamped at the base subjected to a uniformly distributed load perpendicular to its axis line, a rough representation of inertia forces prior to cracking that can be at first stage accepted due to the very small deflections the wall undergoes up to this point (Doherty 2000). Further parameters are the self weight, and the axial superimposed load. Moreover, let us assume that the mortar in the bed joints has a uniformly distributed tensile strength f_{mt}, which can be made non dimensional through the stress induced by the wall self weight: $t = f_{mt}/(W/2b)$. Under the previous assumptions, it is possible to show that the height where the first crack develops if,
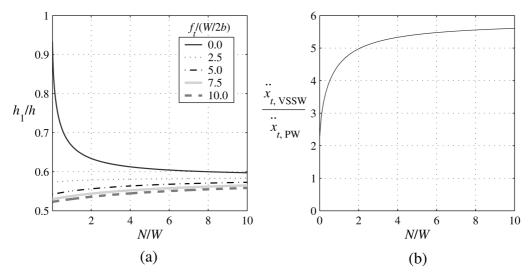
Fig. 3 (a) Non dimensional intermediate hinge height as a function of non dimensional superimposed load and mortar tensile strength, (b) Ratio between threshold accelerations of two walls differing only for the top restraint: absent (PW) or present (VSSW)

after cracking at the base, a redistribution among horizontal reactions takes place, is equal to

$$\frac{h_1}{h} = 1 + \frac{\xi + t - \sqrt{(2 + t + 2\xi)(t + \xi)}}{2 + \xi} \tag{16}$$

A plot of Eq. (16) is presented in Fig. 3(a). It is clear that very small values of mortar tensile strength are sufficient to let the hinge migrate much lower, thus t plays an important role in the response of the system although it does not explicitly appear in the equation of motion as the superimposed load N does. Values of t in ABK (1981) spanned from 5 to 21, while in Doherty (2000) varied between 7 and 9. It should be noted that in Wilhelm *et al.* (2007) t was equal, on average, to 1.6, thus contributing to explain the observations about the crack position. For large values of t and no superimposed load the hinge location tends towards the wall mid-height ($h_1/h = 0.5$), while for both t and ξ increasing the asymptotic limit of Eq. (16) is again $2 - \sqrt{2}$. Moreover, the difference between the curve for $t = 0$ in Fig. 3(a) and a plot of Eq. (15) is negligible.

Irrespective of the assumed model, it is very difficult to exactly predict the hinge height due to mortar tensile strength variability and precracking that may occur during the construction and curing stages, thermal stresses, foundation settlements, and so on. Experimental tests have shown that it is usually positioned at 50-70% of the wall's height (refer to Table 1, Simsir *et al.* 2004, Meisl *et al.* 2006, Wilhelm *et al.* 2007). Nonetheless, for those interested in performing nonlinear time history analyses (Meisl *et al.* 2006, Goretti *et al.* 2007), Eq. (16) is a tool to estimate intermediate hinge height based on the wall characteristics.

In order to highlight some characteristics of the VSSW it is useful to compare it to a free standing or parapet wall (PW), that is a wall whose top has no significant displacement restriction. By modelling the PW as a rigid rocking body it is possible to extract a wealth of information since the so-called Housner inverted pendulum has been extensively studied in the last decades (e.g., refer to: Sorrentino *et al.* 2006).

Let us assume to compute the intermediate hinge of the VSSW position through Eq. (14), with h_1/h

defined by Eq. (15). It is possible to compute the threshold acceleration for the PW from simple statics using Eq. (17)

$$|\ddot{x}_t|_{PW} = \frac{b}{h}g(1 + \xi)$$ (17)

The ratio between the threshold accelerations for a VSSW and PW can be written as

$$\frac{|\ddot{x}_t|_{VSSW}}{|\ddot{x}_t|_{PW}} = 3 + 2\sqrt{\frac{2\xi}{1 + \xi}} - \frac{1}{1 + \xi}$$ (18)

Considering the two walls equal (same b and h refer to Fig. 1(a)) except for the top restraint condition, the threshold acceleration of the VSSW is of course higher than that of a PW. The difference is greater for increasing values of non dimensional load ξ, since the latter causes the hinge to form lower and lower. Nonetheless, due to the limit of Eq. (15), the ratio of the two accelerations, after a rapid growth, approaches the limit of $3 + 2\sqrt{2} \cong 5.83$ (refer to Fig. 3(b)).

5. Energy dissipation

Until now no energy dissipation has been considered. The hypothesis that will be assumed is that, as in other rocking systems (Housner 1963, Spanos *et al.* 2001), energy is damped only when an impact occurs. Due to the restraint conditions, when the lower body hits the ground the former is hit by the upper one. Depending upon the boundary conditions, a VSSW could have two impact sections (cracks) closing whereas a PW has only one. The amount of kinetic energy dissipated can be computed by means of the usual assumptions of impulsive dynamics. These are: infinitesimal impact duration, no variation in the configuration, instant variation in velocity. Moreover, elastic rebound will be excluded; that is, after the impact the rotation corner will change, and it will be assumed that the impact impulse will pass through the rotation hinge. Since the impact duration is infinitesimal, the contributions of body weights, restraint reactions, and the eventual superimposed load to angular momentum are negligible, whilst the inner impact impulses vanish due to the third law of Newton's mechanics. Therefore, if angular momentum is computed with respect to the rotation hinge it will be conserved. Thus, equating the angular momentum before and after the impact it will be possible to compute the energy dissipation.

Recurring to Eqs. (5a and b), and equating the angular momentum after and before the impact it is possible to write down the ratio e between angular velocities after, superscript $^+$, and before, superscript $^-$, the impact

$$\frac{\dot{\theta}_1^+}{\dot{\theta}_1^-} = e = \frac{m_1 R_1^2 + I_{G,1} - I_{G,2}\dfrac{\tan\alpha_2}{\tan\alpha_1} - 2m_1 R_1^2\sin^2\alpha_1 + m_2 R_1^2\left[2 + \dfrac{\sin\alpha_1\cos\alpha_1}{\tan\alpha_2} - \sin^2\alpha_1\left(4 + \dfrac{\tan\alpha_2}{\tan\alpha_1}\right)\right]}{m_1 R_1^2 + I_{G,1} - I_{G,2}\dfrac{\tan\alpha_2}{\tan\alpha_1} + m_2 R_1^2\left[2 + \sin\alpha_1\cos\alpha_1\left(\dfrac{1}{\tan\alpha_2} + \tan\alpha_2\right)\right]}$$ (19)

"e" is usually called the coefficient of restitution, although the term is more appropriate for impact involving points rather than finite surfaces (Shenton and Jones 1991). For homogenous bodies and for an intermediate hinge at mid-height it is possible to simplify Eq. (19). Various plots of the coefficient of restitution are presented in Fig. 4. Therein it is clear that e is more sensitive to α_1 than to α_2. Such behaviour is due to the asymmetry of the mechanism, whose upper body vertical
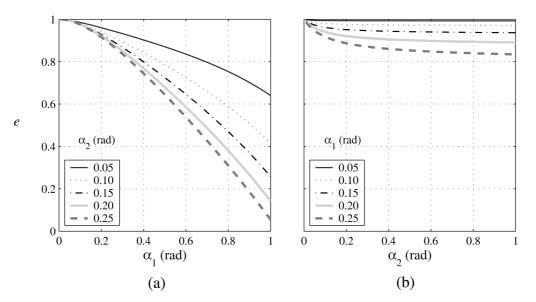
Fig. 4 Coefficient of restitution e varying α_1 (a) and α_2 (b)
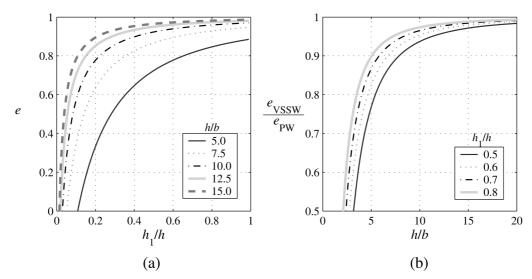

Fig. 5 (a) Coefficient of restitution varying non dimensional intermediate hinge height and wall height to thickness ratio. The practical range of interest of the abscissa is between 0.5 and 0.7. (b) ratio of coefficients of restitutions of a VSSW and of a PW, differing only for the top restraint condition, for various height to thickness ratios, and for different VSSW intermediate hinge heights

component of motion is affected by the rotation of the lower one. Furthermore, it is interesting to note that the plot of e versus α_1 is qualitatively similar to the one of e versus α in a single rocking body (Yim *et al.* 1980).

For a given wall the coefficient of restitution will decrease, (i.e., damping increases) for stockier (larger α) walls and the lower the intermediate hinge (higher N) (Fig. 5(a)). Therefore it is clear that the superimposed gravity load as well as the tensile strength, although not present in Eq. (19)), play
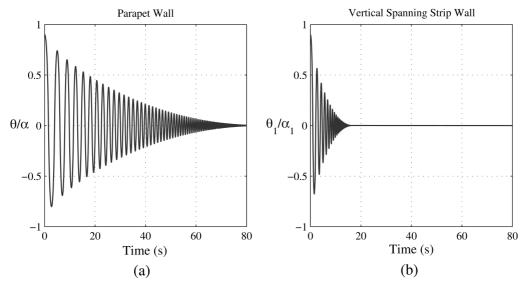
Fig. 6 Free vibrations of a parapet wall (a) and of a vertical spanning strip wall (b), differing only for the top restraint condition. $b = 0.2$ m, $h = 2$ m, $\xi = 0$, $h_1/h = 0.7$, $\theta_0/\alpha = \theta_{1,0}/\alpha_1 = 0.9$, $\dot{\theta}_0 = \dot{\theta}_{1,0} = 0$

a role in energy absorption by positioning the hinge height.

A comparison between the coefficient of restitution of two walls, equal in all except for the top restraint condition, is presented in Fig. 5(b). Therein it is possible to observe that the coefficient of restitution of a vertical spanning strip wall is always lower than that of a parapet wall. Nevertheless, the difference between the two conditions decreases as a wall becomes more slender and/or the intermediate hinge moves up. The reduction of e that the passage from a PW to a VSSW involves can markedly reduce the free vibration duration of two walls with same size and height to thickness ratio (same b and h), as well as initial conditions (Fig. 6). PW free vibrations are computed using the nonlinear Housner (1963) model, while VSSW ones are obtained from Eq. (10). In both cases numerical integration has been carried out in a state-space formulation using a Runge-Kutta algorithm of variable order and time step (The Mathworks 2003), whose default error tolerances have been reduced (Sorrentino *et al.* 2006). After being released, the VSSW stops in less than a quarter of the time required by the PW (Fig. 6).

Such higher energy dissipation capacity has a laboratory confirmation. As a matter of fact, Lam *et al.* (1995), after an experimental campaign on unreinforced masonry parapet walls of 0.9 m rocking height and 0.11 m thickness, proposed a 3% equivalent viscous damping ratio, while Doherty (2000), after testing vertical spanning strip walls likewise built, but with a 1.5 m height (thus more slender), and with an intermediate hinge near mid height, suggested a value of 6%. As remarked by these authors and as will be shown in the next section, energy dissipation through coefficient of restitution is amplitude dependent. However, it is possible to estimate an equivalent viscous damping ratio from logarithmic decrement of free vibrations, computed analogously to those of Fig. 6. Starting in both cases from a non dimensional initial rotation equal to 0.7, the values calculated after four cycles are 3.0% for the Lam *et al.* wall and 6.5% for the Doherty *et al.* wall.

Therefore, the addition of the top restraint not only increases the collapse static load multiplier (refer to § 4) but it also enhances the energy dissipation capacity of the system, as observed for other rocking systems (Makris and Black 2002). Moreover, in this case damping appears to be more

related to the mechanism than the material. This is a further difference between rocking and elastic oscillators. Finally, this dynamic analysis proves highly valuable in delivering information that is otherwise not available from pure static analysis. For those interested in performing nonlinear time history analyses (Wilhelm *et al.* 2007, Goretti *et al.* 2007), Eq. (19) is a tool to estimate energy dissipation based on the wall characteristics.

6. Amplitude dependency of energy dissipation and period of vibration

An explanation of the increase in damping due to increasing displacements can be gained by considering the linearised equation for free vibrations when the superimposed load N is absent

$$\ddot{\theta}_1 = -\text{sgn}(\theta_1)P^2(A - |\theta_1|) \tag{20}$$

with

$$A = \frac{\alpha_1\left[m_1 + m_2\left(2 + \dfrac{\cos\alpha_1}{\cos\alpha_2}\dfrac{\alpha_2}{\alpha_1}\right)\right]}{m_1 + m_2\left(2 + \dfrac{\cos\alpha_1}{\cos\alpha_2}\dfrac{\tan\alpha_2}{\tan\alpha_1}\right)} \tag{21a}$$

$$P^2 = \frac{g\left[m_1 + m_2\left(2 + \dfrac{\cos\alpha_1}{\cos\alpha_2}\dfrac{\tan\alpha_2}{\tan\alpha_1}\right)\right]}{R_1\left\{m_1 + m_2\left[\cos^2\alpha_1 + \sin^2\alpha_1\left(2 + \dfrac{\tan\alpha_2}{\tan\alpha_1}\right)^2\right] + \dfrac{1}{R_1^2}\left[I_{G,1} + I_{G,2}\left(\dfrac{\tan\alpha_2}{\tan\alpha_1}\right)^2\right]\right\}} \tag{21b}$$

Eq. (20) has the same form of that of single rocking body in free vibrations (Housner 1963), with the parameter A being equivalent to the angle α. From Eq. (21a) it is evident that $A \cong \alpha_1$ in the practical range of values of α_1 and α_2. Since the coefficient of restitution of a single rocking body is a function of α (Housner 1963), the top restraint, by increasing its value, increases the energy dissipation.

Integrating Eq. (20) in closed form it is possible to compute the period of free vibration, T, based on one quarter of a cycle

$$T = \frac{4}{P}\text{arccosh}\left(\frac{1}{1 - \dfrac{\theta_{1,0}}{A}}\right) \tag{22}$$

with $\theta_{1,0}$ being the initial rotation of the system. A plot of Eq. (22) is presented in Fig. 7(a), where it is compared to the analogous plot for the Housner rocking block. The amplitude dependency has the same shape, however the introduction of the upper restraint involves a reduction of the period. The latter is a function of the aspect ratio and the position of the intermediate hinge (Fig. 7(b)), not of the size of the system nor the amplitude of motion.

As previously mentioned, it is possible to prove that energy dissipation is amplitude dependant. When a VSSW in free vibrations gets its maximum rotation all its energy is potential, whereas at
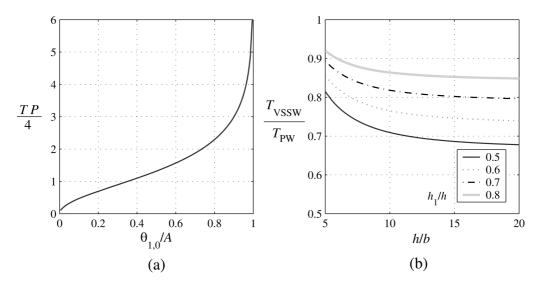
Fig. 7 (a) Non dimensional period of vibration of Vertical Spanning Strip Wall as a function of non dimensional amplitude of the motion, (b) ratio between the periods of a Vertical Spanning Strip Wall and a Parapet Wall as a function of aspect ratio and non dimensional intermediate hinge height. $N/W = 0$
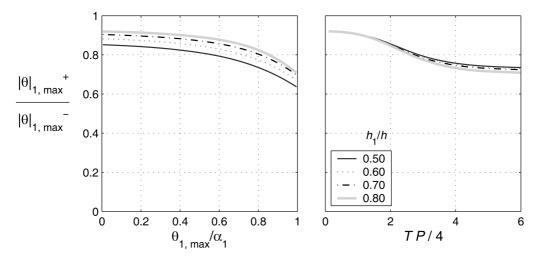

Fig. 8 Ratio between two peak angular displacements, one half cycle apart, as a function of non dimensional amplitude of motion. $h/b = 10$

the impact the energy is fully kinetic, if potential energy is measured from rest position. In such time interval it is possible to resort to the principle of energy conservation, since under the assumed hypothesis, energy dissipation is concentrated at impacts. Therefore, assigned the coefficient of restitution it is possible to plot the ratio between two (absolute) peak angular displacements, one half cycle apart. A sample plot is presented in Fig. 8(a), where it is evident that the higher the amplitude the higher the damping in agreement to what has been experimentally observed (Doherty 2000). In Fig. 8(b) the dependency upon the non dimensional period of vibration is highlighted by means of Eq. (22).

Moreover, the same concept can be used to measure an experimental coefficient of restitution when displacements, not velocities, have been surveyed. Equating potential and kinetic energies it is possible to express the coefficient of restitution as a function of the amplitude of rotation before and after the impact. Hence, by means of Eqs. (6), (7) and (11a-b) one gets

$$
e = \sqrt{\frac{\left\{\dfrac{(m_1 + 2m_2)(\cos A_1^+ - \cos \alpha_1) + m_2 \dfrac{\sin \alpha_1}{\sin \alpha_2}(\cos A_2^+ - \cos \alpha_2)}{m_1 + m_2\left[\cos^2 A_1^+ + \sin^2 A_1^+\left(2 + \dfrac{\tan A_2^+}{\tan A_1^+}\right)^2\right] + \dfrac{1}{R_1^2}\left(I_{G,1} + \dfrac{\sin^2 \alpha_2 \cos^2 A_1^+}{\sin^2 \alpha_1 \cos^2 A_2^+}I_{G,2}\right)}\right\}}{\left\{\dfrac{(m_1 + 2m_2)(\cos A_1^- - \cos \alpha_1) + m_2 \dfrac{\sin \alpha_1}{\sin \alpha_2}(\cos A_2^+ - \cos \alpha_2)}{m_1 + m_2\left[\cos^2 A_1^- + \sin^2 A_1^-\left(2 + \dfrac{\tan A_2^-}{\tan A_1^-}\right)^2\right] + \dfrac{1}{R_1^2}\left(I_{G,1} + \dfrac{\sin^2 \alpha_2 \cos^2 A_1^-}{\sin^2 \alpha_1 \cos^2 A_2^-}I_{G,2}\right)}\right\}}} \qquad (23)
$$

with $A_1^{\pm} = \alpha_1 - \left|\theta_{1,\max}^{\pm}\right|$, $A_2^{\pm} = \alpha_2 - \dfrac{\tan \alpha_2}{\tan \alpha_1}\left|\theta_{1,\max}^{\pm}\right|$.

7. Sample time histories. Scale effect

The response of the VSSW to four seismic ground motions has been evaluated. Information about the four recorded accelerograms used is reported in Table 2.

Time history results presented in Fig. 9 include plots of non dimensional rotation, angular velocity, mechanical (i.e., potential plus kinetic) and dissipated energies. The displacement has been normalised by angle α_1, where a value of unity corresponds to the instability threshold under gravity

Table 2 Recorded accelerograms used and their main features

	Event	Date	M_W[a]	Station	D[c] km	Soil[d]	PGA[e] g	PGV[e] cm/s	PGD[e] cm	Δt[f] s	Record
1	Romania	1977-III-4	7.5	Bucarest, Romania Building Research Institute	150	S3	0.21	73.6	24.4	16.2	Bucar0
2	Irpinia, Italy	1980-XI-23	6.8[b]	Calitri	20.7	S2	0.18	18.7	5.1	68.9	CalitWE
3	Northridge, CA, USA	1994-I-17	6.7	Rinaldi Receiving Station	0.1	S2	0.84	166.1	28.8	14.945	RRS228
4	ChiChi, Taiwan	1999-IX-20	7.6	TCU129	1.2	S1	1.01	60	50.4	89.995	TCU129W

[a]M_W = moment magnitude.
[b]M_S = surface waves magnitude.
[c]D = Distance from the surface projection of the source.
[d]Soil: S1 = stiff, S2 = intermediate, S3 = soft (Decanini and Mollaioli 1998).
[e]Peak Ground: PGA = Acceleration, PGV = Velocity, PGD = Displacement.
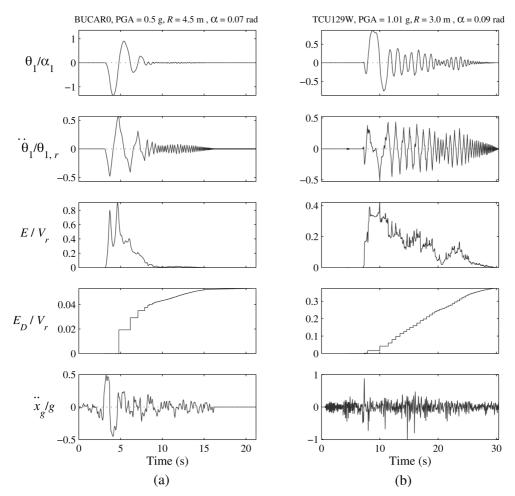[f]Δt = Duration.

Fig. 9 Sample time histories of, from top to bottom, normalised angular displacement and velocity, mechanical energy, dissipated energy and ground acceleration. $N/W = 0.1$, $h_1/h = 0.6$. Amplitudes of accelerogram (a) are scaled

forces alone. Velocity was normalised by the reference angular velocity $\dot{\theta}_{1,r}$

$$\dot{\theta}_{1,r} = \sqrt{\frac{2g\left[\left(m_1 + 2m_2 + 2\frac{N}{W}W\right)(1-\cos\alpha_1) + \left(m_2 + 2\frac{N}{W}W\right)\frac{\sin\alpha_1}{\sin\alpha_2}(1-\cos\alpha_2)\right]}{R_1\left\{m_1 + m_2\left[\cos^2\alpha_1 + \sin^2\alpha_1\left(2 + \frac{\tan\alpha_2}{\tan\alpha_1}\right)^2\right] + \frac{1}{R_1^2}\left[I_{G,1} + I_{G,2}\left(\frac{\tan\alpha_2}{\tan\alpha_1}\right)^2\right]\right\}}} \quad (24)$$

this being the velocity that brings a resting VSSW to the position $\theta_1 = \alpha_1$. Mechanical energy, E, and the cumulated dissipated energy (sum of the kinetic energy lost at every impact), E_D

$$E_D = \frac{1}{2}R_1\left\{m_1 + m_2\left[\cos^2\alpha_1 + \sin^2\alpha_1\left(2 + \frac{\tan\alpha_2}{\tan\alpha_1}\right)^2\right] + \frac{1}{R_1^2}\left[I_{G,1} + I_{G,2}\left(\frac{\tan\alpha_2}{\tan\alpha_1}\right)^2\right]\right\}(1-e^2)\sum_i(\theta_{1,i}^-)^2 \quad (25)$$

were both normalised by the difference in potential energy, V_r, between the values for $\theta_1 = \alpha_1$ and $\theta_1 = 0$.

As noted elsewhere for a simple rocking body (Sorrentino *et al.* 2006), the rotation is closely related to overturning of the system, with non dimensional velocity and mechanical energy more easily exceeding the unity threshold without collapse. This is especially true if the system is very slender (small α) and relatively tiny because its potential energy is a minor fraction of the input energy. As a matter of fact, in these cases it is the driving force that brings the system back to a bounded oscillation. Sometimes the normalised displacement can also show this kind of behaviour (Fig. 9(a)). Nonetheless, such occurrences are far less frequent than in a PW due to the presence of the superimposed load which induces a pronounced P-Δ effect. However, this requires integration to be performed up to the violation of the top restraint, i.e., when the distance between the intermediate hinge and normal to the roller support axis equals the diagonal of the upper body ($2R_2$). This happens for a limit rotation $\theta_{1,\,\text{lim}}$

$$\theta_{1,\,\text{lim}} = \arcsin\left(\frac{\sin\alpha_1}{\sin\alpha_2}\right) + \alpha_1 \tag{26}$$

In Fig. 10 a plot of the maximum absolute rotations for a set of VSSW is presented. For the sake of representation, α values start from zero (corresponding theoretically to an infinitely slender VSSW), assuming fictitiously values of unity for normalised displacement, velocity and mechanical energy and zero dissipated energy. As for the Housner inverted pendulum, it is possible to observe, at least in a statistical sense, that the stockier (i.e., higher α) and the bigger (i.e., higher R) the VSSW system the lower its response. However, the latter phenomenon, also known as "scale effect", can vary significantly with the excitation as the comparison of Figs. 10(a) and (b) highlights. As proved for a single rocking body (Sorrentino *et al.* 2006), such differences are due to the difference in potential energy V_r, with the potential energy being defined in Eq. (6). V_r, is a
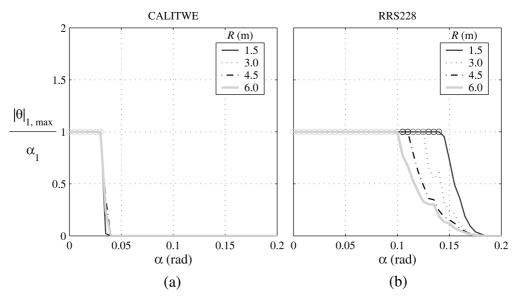

Fig. 10 Rocking curves of VSSW as a function of α and R in terms of normalised maximum absolute rotation for different accelerograms. The circle indicates an overturning. $N/W = 0.1$, $h_1/h = 0.6$
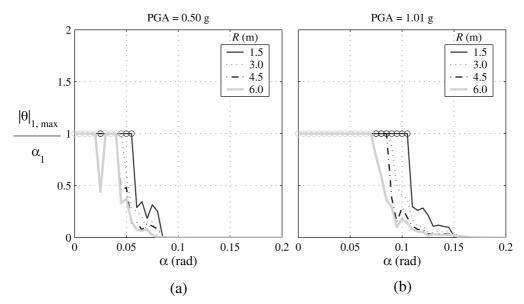
Fig. 11 Maximum absolute rotations response plots to the same accelerogram, TCU129W, with PGA scaled (a) and unscaled (b). The circle indicates an overturning. $N/W = 0.1$, $h_1/h = 0.6$

measure of the energy that is necessary to bring a resting VSSW to the instability ($\theta_1 = \alpha_1$) position. For example, let us consider two systems with identical aspect ratio, nondimensional intermediate hinge height and superimposed load, but different size, R. V_r increases as α increases (i.e., the two walls become stockier). However, to set into motion a stockier wall, the amplitude of the signal needs to be higher. Hence, the scale effect is more noticeable for accelerograms with high amplitude. This is also observed when comparing the responses for the same record but at differing amplitudes: the curves of equal size R begin to differ significantly once the accelerations increase (compare Figs. 11(a) to 11(b)). Therefore, the "scale effect" is expected to be more significant in higher seismicity areas than in lower ones. The Italian Seismic Code (OPCM 2005, annex 11.C) currently accounts for this scale effect in the check against local mechanisms in existing unreinforced masonry buildings. However, it does not differentiate the role of the size of the wall in the different seismic zones, as it should based on what has been highlighted here and elsewhere (Sorrentino *et al.* 2006).

8. Conclusions

The equation of motion for a vertically spanning strip wall has been presented. If the system is homogenous, it can be fully described by three geometrical parameters (α_1, α_2 and R_1, or b, h_1 and h_2), its mass density, and the superimposed gravity load N. Furthermore, it has only one degree of freedom: the rotation of the lower body.

The nonlinear equation of motion, with non constant coefficients and a Coriolis acceleration, was derived under the assumptions that α_1 is small or tends to α_2 (as observed in both field and laboratory tests), no slip occurs, the centre of mass of each body is coincident with the geometrical centre, and the two bodies are perfect rectangles.

The latter hypothesis involves the existence of a threshold acceleration necessary to trigger rocking motion. Such acceleration depends only on the shape (α_1, α_2), the density, and N, but not on the size of the wall. With the exception of the position of the intermediate hinge, all these parameters are measurable. The hinge location cannot be precisely predicted, as previous experimental tests confirm. Both the intensity of N, compared to the wall's self weight, and the tensile strength play a role in determining hinge location. An analytical formulation has been suggested in this paper, which shows that the hinge position is lower for higher N and tensile strength, and which is useful to perform time history analyses. Irrespective of the height of the intermediate crack, the addition of the top restraint causes an increase of the threshold acceleration of the vertical spanning strip wall compared to that of a simple standing, or parapet, wall.

Significantly, this is not the only benefit of having a top restraint. In fact, modelling energy damping by means of impulsive dynamics has shown that the dissipation of energy in a vertical spanning strip wall is higher than in a parapet wall of equal size and shape. This phenomenon, already reported in the literature after experimental tests, was theoretically explained in this paper, and an equation to assess the so-called coefficient of restitution has been proposed. The similarity between a VSSW and a PW holds even when it comes to energy dissipation and period of vibration dependency upon amplitude of vibration. A closed form relationship has been derived for the linearised free-vibration equation of motion. This shows that both damping and period increases, in a non-linear way, as the amplitude increases which is in agreement with experimental data. A few sample time histories have been computed, showing again a similarity to those of a single rocking body. Again, a VSSW proves safer the stockier (larger α) and the bigger (larger R) it is. The latter behaviour, also known as scale effect, is however more evident with high amplitude accelerograms because the difference in the energy that is necessary to overturn two walls with same shape but different size builds up the stockier they are. Therefore, scale effect is expected to be noticeable in high seismicity areas.

Aknowledgements

References

ABK (1981), *Methodology for Mitigation of Seismic Hazards in Existing Unreinforced Masonry Buildings: Wall Testing, Out of Plane. Topical Report 04*, Agbabian Associates, El Segundo, CA, USA.

ABK (1984), *Methodology for Mitigation of Seismic Hazards in Existing Unreinforced Masonry Buildings: The Methodology. Topical Report 08,* Agbabian Associates, El Segundo, CA, USA.

Allen, R.H., Oppenheim, I.J., Parker, A.R. and Bielak, J. (1986), "On the dynamic response of rigid body assemblies", *Earthq. Eng. Struct.*, **14**(6), 861-876.

Anderson, C. and Held, L. (1982), "The stability of cracked walls subjected to lateral loading", *Proc. of the 6th Int. Brick Masonry Conf.,* Rome, Italy.

Baggio, C. and Masiani, R. (1991), "Dynamic behaviour of historical masonry", *Proc. of the 9th Int. Brick/Block*

Masonry Conf., Berlin, Germany.

Decanini, L.D. and Mollaioli, F. (1998), "Formulation of elastic earthquake input energy spectra", *Earthq. Eng. Struct.*, **27**(12), 1503-1522.

Doherty, K.T. (2000), *An Investigation of the Weak Links in the Seismic Load Path of Unreinforced Masonry Buildings, PhD Dissertation*, School of Civil and Environmental Engineering, The Adelaide University, Adelaide, Australia.

Doherty, K.T., Griffith, M.C., Lam, N.T.K. and Wilson, J.L. (2002), "Displacement-based seismic analysis for out-of-plane bending of unreinforced masonry walls", *Earthq. Eng. Struct.*, **31**(4), 833-850.

Giuffrè, A. (ed) (1993), *Sicurezza e conservazione dei centri storici: il caso Ortigia*, Laterza, Roma-Bari, Italy, 183-184 and 229-256.

Goretti, A., De Matteis, U. and Liberatore, D. (2007), "Analisi Sismica delle Mura Storiche di Camerino", *Proc. of the 12th Convegno nazionale "L'ingegneria sismica in Italia"*, Pisa, Italy.

Griffith, M.C., Lam, N.T.K., Wilson, J.L. and Doherty, K.T. (2004), "Experimental investigation of URM walls in flexure", *J. Struct. Div.*, ASCE, **130**(3), 423-432.

Griffith, M.C., Magenes, G., Melis, G. and Picchi, L. (2003), "Evaluation of out-of-plane stability of unreinforced masonry walls subjected to seismic excitation", *J. Earthq. Eng.*, **7**(SI 1), 141-169.

Gülkan, P., Mayes, R.L. and Clough, R.W. (1979), *Shaking Table Study of Single-story Masonry Houses. Vol. 1: Test Structures 1 and 2*, Earthquake Engineering Research Center, Berkeley, CA, USA.

Housner, G.W. (1963), "The behavior of the inverted pendulum structures during earthquakes", *B. Seismol. Soc. Am.*, **53**(2), 403-417.

Ishiyama, Y. (1984), "Motions of rigid bodies and criteria for overturning by earthquake excitations", *B. New Zealand National Soc. Earthq. Eng.*, **17**(1), 24-37.

Koh, A.S., Spanos, P.D. and Roesset, J.M. (1986), "Harmonic rocking of rigid block on flexible foundation", *J. Eng. Mech.*, ASCE, **112**(11), 1165-1180.

Lam, N.T.K., Griffith, M.C., Wilson, J.L. and Doherty, K.T. (2003), "Time-history analysis of URM walls in out-of-plane flexure", *Eng. Struct.*, **25**(6), 743-754.

Lam, N.T.K., Wilson, J.L. and Hutchinson, G.L. (1995), *Modelling of an Unreinforced Masonry Parapet Wall for Seismic Performance Evaluation based on Dynamic Testing*. Department of Civil and Environmental Engineering, University of Melbourne, Melbourne, Australia.

Makris, N. and Black, C. (2002), "Uplifting and overturning of equipment anchored to a base foundation", *Earthq. Spectra*, **18**(14), 631-661.

Meisl, C.S., Elwood, K.J., Mattman, D.W. and Ventura, C.E. (2006), "Out-of-plane seismic performance of unreinforced clay brick masonry walls", *Proc. of 8th U.S. National Conf. on Earthquake Engineering*, San Francisco, CA, USA.

OPCM (Ordinanza del Presidente del Consiglio dei Ministritri (OPCM) no. 3431 del 3 maggio 2005. Ulteriori modifiche e integrazioni all'OPCM n.3274 del 20 marzo 2003. *Gazzetta Ufficiale* n.107 del 10 maggio 2005. (English translation: http://www.eucentre.it/eng/files/OPCM_Ch8_11_English_ver.pdf)

Oppenheim, I.J. (1992), "The masonry arch as a four-link mechanism under base motion", *Earthq. Eng. Struct.*, **21**(11), 1005-1017.

Psycharis, I.N. (1990), "Dynamic behaviour of rocking two-block assemblies", *Earthq. Eng. Struc.*, **19**(4), 555-575.

Shenton, H.W. III and Jones, N.P. (1991), "Base excitation of rigid bodies. I: Formulation", *J. Struct. Div.*, ASCE, **117**(10), 2286-2306.

Simsir, C.C., Aschheim, M.A. and Abrams, D.P. (2004), "Out-of-plane dynamic response of unreinforced masonry bearing walls attached to flexible diaphragms", *Proc. of the 13th World Conf. on Earthquake Engineering*, Vancouver, BC, Canada.

Sinopoli, A. and Sepe, V. (1993), "Coupled motion in the dynamic analysis of a three block structure", *Appl. Mech. Rev.*, ASME, **46**(11-2), S185-S197.

Sorrentino, L. and Masiani, R. (2003), "Dynamic out-of-plane behaviour of unreinforced masonry walls", *Proc. of the 6th Int. Symposium on Computer Methods in Structural Masonry*, Rome, Italy.

Sorrentino, L., Masiani, R. and Decanini, L.D. (2006), "Overturning of rocking rigid bodies under transient ground motions", *Struct. Eng. Mech.*, **22**(3), 293-310.

Spanos, P.D. and Koh, A.S. (1984), "Rocking of rigid blocks due to harmonic shaking", *J. Eng. Mech.*, ASCE, **110**(11), 1627-1642.

Spanos, P.D. and Koh, A.-S. (1986), "Analysis of block random rocking", *Soil Dyn. Earthq. Eng.*, **5**(3), 178-183.

Spanos, P.D., Roussis, P.C. and Politis, N.P.A. (2001), "Dynamic analysis of stacked rigid blocks", *Soil Dyn. Earthq. Eng.*, **21**(7), 559-578.

The MathWorks Inc. (2003), *MATLAB*, Natick, MA, USA.

Tso, W.K. and Wong, C.M. (1989), "Steady state rocking response of rigid blocks Part 2: Experiment", *Earthq. Eng. Struc.*, **18**(1), 107-120.

Wilhelm, M., Mojsilović, N. and Dazio, A. (2007), "Out-of-plane shaking table tests on unreinforced masonry walls", *Proc. of the 10th North American Masonry Conference,* St. Louis, MO, USA.

Winkler, T., Meguro, K. and Yamazaki, F. (1995), "Response of rigid body assemblies to dynamic excitation", *Earthq. Eng. Struct.*, **24**(10), 1389-1408.

Yim, C.S., Chopra, A. and Penzien, J. (1980), "Rocking response of rigid blocks to earthquakes", *Earthq. Eng. Struct.*, **8**(6), 565-587.